SLAC-PUB-6694
January 1995
(A/E)

POLARIZATION AT SLAC*

M. Woods

Stanford Linear Accelerator Center
Stanford University, Stanford, CA 94309

Abstract. A highly polarized electron beam is a key feature for the current physics program at SLAC. An electron beam polarization of 80% can now be routinely achieved for typically 5000 hours of machine operation per year. Two main physics programs utilize the polarized beam. Fixed target experiments in End Station A study the collision of polarized electrons with polarized nuclear targets to elucidate the spin structure of the nucleon and to provide an important test of QCD. Using the SLAC Linear Collider, collisions of polarized electrons with unpolarized positrons allow precise measurements of parity violation in the Z-fermion couplings and provide a very precise measurement of the weak mixing angle. This paper discusses polarized beam operation at SLAC, and gives an overview of the polarized physics program.

Presented at the Eleventh International Symposium
on High Energy Spin Physics
Bloomington, Indiana USA, September 15-22, 1994

* Work supported in part by the Department of Energy, contract DE-AC03-76SF00515

POLARIZED PHYSICS PROGRAM

1. Fixed-Target Experiments in End Station A (ESA)

The nucleon has spin 1/2, and has a rather complex internal structure that contains valence quarks, sea quarks and gluons. Deep inelastic scattering experiments tell us that about half of a nucleon's momentum is carried by the quarks and about half is carried by the gluons.[1] But how much of the nucleon's spin is due to the quarks, how much is due to the gluons, and how much is due to orbital angular momentum? Measurements of the longitudinal proton spin structure function (g_1^p) by the SLAC experiments E80[2] and E130,[3] and by the CERN EMC experiment,[4] indicated that the quarks contribute only $(12 \pm 17)\%$ of the nucleon spin.[4] This small contribution, consistent with zero, came to be known as the "Spin Crisis" and led to the proposal of new experiments at SLAC, CERN, and DESY.

The Ellis-Jaffe sum rules[5] give predictions for $\int g_1^p dx$ and $\int g_1^n dx$, and are based on SU(3) symmetry and an assumption that the strange sea is unpolarized. Using the quark parton model, $\int g_1^p dx$ and $\int g_1^n dx$ can be used to determine the total quark contribution to the nucleon spin.[6] Bjorken has also developed a sum rule for $\int (g_1^p - g_1^n)dx$, which follows from current algebra.[7] A violation of the Ellis-Jaffe sum rules would imply that the existing model of nucleon structure is too simple. A violation of the Bjorken sum rule would be more serious, and would pose a significant challenge to current QCD theory.

Recently, SLAC experiment E142 has made the first measurement of g_1^n,[8] and E143 has measured g_1 for the proton and deuteron.[9] The CERN SMC experiment has also recently measured g_1 for the deuteron[10] and proton.[11] As summarized in other contributions to this conference,[12] the new experimental data from SLAC and CERN indicate that the Bjorken sum rule is satisfied (less than 1σ discrepancy with the data). However, the Ellis-Jaffe sum rule for the proton appears to be violated (greater than 3σ discrepancy with the data), and the quarks appear to account for only one third of the proton's spin (0.31 ± 0.07).

The g_1 measurements at SLAC will continue with further measurements on the neutron by E154, and on the proton and deuteron by E155 (see Table I for relevant beam parameters and dates for running).

2. The SLD Experiment at the SLAC Linear Collider (SLC)

The Minimal Standard Model (MSM) of electroweak interactions gives the gauge structure of the theory as $SU(2)_L$ X $U(1)$. This gauge structure results in four physical gauge bosons (W^+, W^-, Z^0, γ) that mediate the interactions. Figure 1 shows the Feynman diagrams for the different gauge boson - fermion vertices and gives the couplings of these vertices separately for left- and right-handed fermions. It is clear from this figure that electroweak interactions treat left-handed and right-handed fermions differently.

The charged W couples *only* to left-handed fermions; the photon couples *equally* to both; and the Z couples to both, but *asymmetrically*. For the Z-fermion coupling, one can

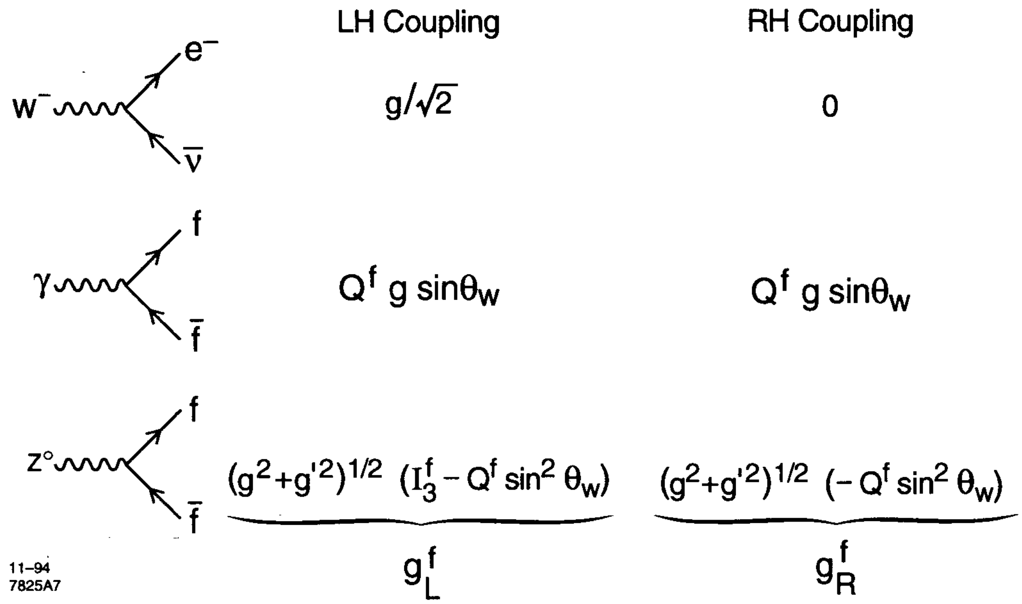

Figure 1. Left and right couplings at the gauge boson- fermion vertices. The $\mathbf{SU(2)}_L$ coupling constant is g; g' is the U(1) coupling constant; Q^f is the fermion charge; I_3^f is the fermion isospin component; and θ_w is the weak mixing angle ($\tan\theta_w \equiv g'/g$).

define the following asymmetries,

$$A_f \equiv \frac{(g_L^f)^2 - (g_R^f)^2}{(g_L^f)^2 + (g_R^f)^2}$$

These asymmetries are large. For example, A_e is expected to be about 15%.

The SLC is currently operating with e^+e^- collisions at the Z^0 resonance. The availability of a highly polarized electron beam gives the capability for direct measurements of the asymmetries A_f. These are now being measured by the SLD detector.[13,14]

In particular, the SLD is making a very precise measurement of the left-right asymmetry,

$$A_{LR} \equiv \frac{\sigma(e_L^- e^+ \to Z^0) - \sigma(e_R^- e^+ \to Z^0)}{\sigma(e_L^- e^+ \to Z^0) + \sigma(e_R^- e^+ \to Z^0)} = A_e$$

This measurement[14] now gives the world's best single determination of the weak mixing angle, $\sin^2\theta_W^{\mathrm{eff}}$,[15] and provides one of the best tests of the MSM.[16] The current SLD run is expected to reduce its error on $\sin^2\theta_W^{\mathrm{eff}}$ by a factor of 2.

POLARIZED BEAM OPERATION

1. Polarized Source[17]

Polarized electrons are produced by photoemission from a GaAs photocathode as shown in Figure 2. Different laser light sources are used for the ESA and SLC physics programs due to the different pulse structures required (see Tables I and II). For ESA, a flashlamp-pumped Ti:sapphire laser[18] is used to produce a 2 μs pulse. For SLC operation, two Nd:YAG-pumped Ti:sapphire lasers[19] produce two 2 ns pulses separated by about 60 ns. One of these pulses is used to make electrons for collisions, and the other one is used to make electrons for positron production.

The laser beams are circularly polarized by a linear polarizer followed by a Pockels Cell operating at its quarter-wave voltage. A positive HV pulse on the Pockels Cell produces one helicity, while a negative HV pulse produces the opposite helicity. The sign of the HV pulse is set by a pseudo-random number generator, which updates at 120 Hz (the SLAC machine pulse rate). This very effectively minimizes false experimental asymmetries.

The photoexcitation of electrons in the GaAs cathode from its valence band to the conduction band is illustrated in Figure 3. Consider first the situation for unstrained GaAs in Figure 3a. Photons with positive helicity and with energies greater than the band-gap energy of 1.43 eV, but less than 1.77 eV, can excite the two indicated solid transitions from the $j = 3/2$ valence band to the $j = 1/2$ conduction band. Clebsch-Gordon coefficients give the relative probability for these two transitions to be 3:1. Thus, positive helicity light will produce negative helicity electrons with a net theoretical polarization of 50% ($P = \frac{3-1}{3+1}$). The extracted electrons from the GaAs cathode, however, will have the same helicity as the incident photons since they have opposite direction to the incident photons.

If one splits the $j = 3/2$ valence band degeneracy as shown in Figure 3b, one can theoretically produce an electron beam with polarization close to 100%. In practice this can be accomplished by growing a thin layer of GaAs on GaAsP. The lattice mismatch between the two results in a strained GaAs lattice, which indeed breaks the degeneracy.[20] Such cathodes are now commercially available and have demonstrated polarizations in excess of 80%. The quantum efficiency (emitted electrons per incident photon), QE, of such cathodes is typically 0.2%.

2. Beam and Spin Transport

<u>End Station A Operation.</u> Figure 4 illustrates the beam and spin transport from the polarized source to the End Station A experiments. The electron beam energy at the source is 60 keV. The beam is injected at this energy into the 3-km SLAC linac, where it is bunched and accelerated to energies as high as 29 GeV. (The ESA beam line is currently being upgraded to transport beams with energies up to 50 GeV for experiments E154 and E155.)

The electron spin is longitudinal at the source and remains longitudinal upon injection into the linac. At the end of the linac the beam is deflected with horizontal bend magnets by an angle, θ_b, of 428 mrad into the ESA beam line. This deflection causes the spin to

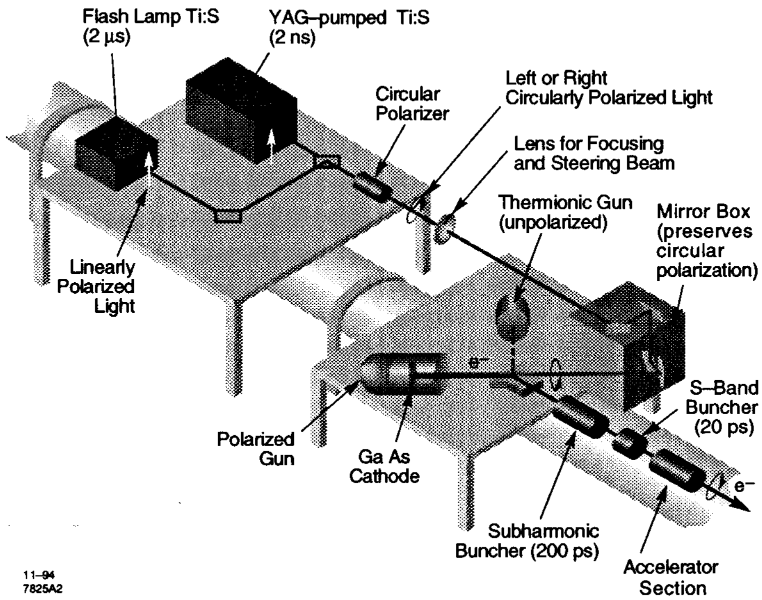

Figure 2. The Polarized Electron Source at SLAC.

precess with respect to the momentum vector by $\Delta\theta = (\frac{g-2}{2})\gamma\theta_b$. When $\Delta\theta = n\pi$ the spin is longitudinal in ESA; this is achieved at beam energies of $E_b = n \cdot 3.24$ GeV. The polarized beam electrons are scattered by the polarized target and are detected in two spectrometers as shown in Figure 4. The polarized electron beam and polarized nuclear target can be set up to have their relative spins longitudinally aligned either parallel or anti-parallel. From the measured cross-section-asymmetry for these two cases, the nucleon spin structure functions (g_1) can be determined.

Table I: Beam Parameters for ESA Operation

Parameter	E142	E143	E154	E155
N^-	$2 \cdot 10^{11}$	$4 \cdot 10^9$	$2 \cdot 10^{11}$	$4 \cdot 10^9$
f_{rep}	120 Hz	120 Hz	120 Hz	120 Hz
Pulse Length	1us	2us	100ns	100ns
Beam Energy	22.7 GeV	29.2 GeV	48.6 GeV	48.6 GeV
Polarization	40%	84%	80%	85%
Run time	2 months	3 months	2 months	3 months
Year	1992	1993	1995	1996

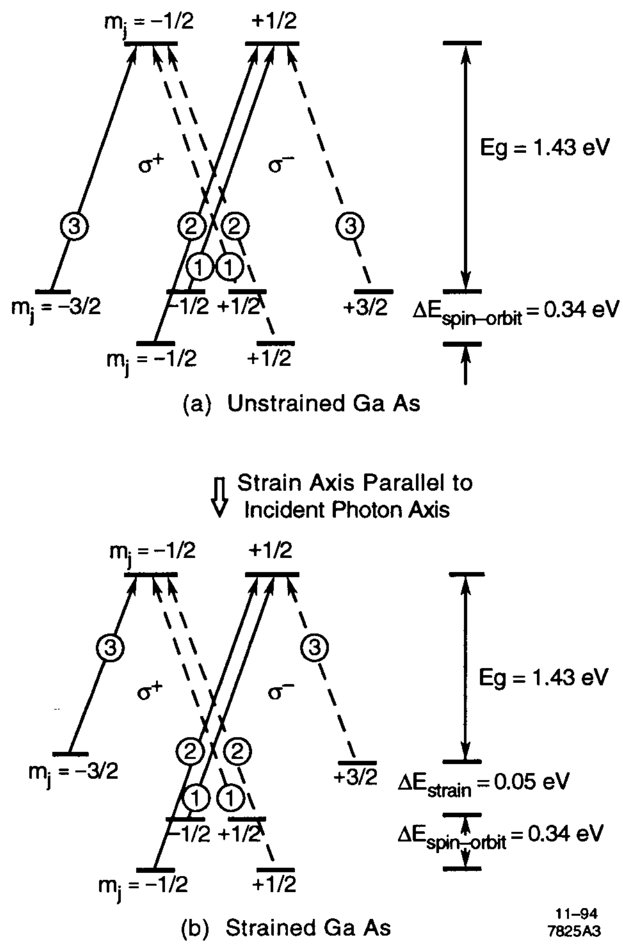

Figure 3. GaAs energy levels and allowed transitions from the valence band to the conduction band. Solid lines indicate transitions due to positive helicity photons. Dashed lines indicate transitions due to negative helicity photons. Circled numbers indicate relative probabilities of transitions.

<u>SLAC Linear Collider Operation.</u> The beam and spin transport are each considerably more complex for SLC operation, as is shown in Figure 5. Two electron bunches are produced from the photocathode gun, which operates at 120 kV. The higher voltage (higher than the 60 kV required for ESA operation) is needed to increase the *space-charge-limit* current capability of the gun above the 6 amps of peak current required for SLC operation. During early operation of the polarized gun for SLC, an unexpected cathode *charge limit* was observed below the space charge limit.[21] The cathode charge limit was observed to be proportional to the cathode quantum efficiency and posed a worry for achieving the needed high currents at the low QEs of the strained lattice cathodes. Similar behavior of the charge limit is indeed observed with the strained lattice cathodes, but the QE scaling factor is different and adequate QEs can be achieved for the SLC current requirements.[22]

The two electron bunches produced from the photocathode gun are injected into the SLAC linac where they are bunched and accelerated to 1.19 GeV. They are then kicked by a pulsed magnet into the linac-to-ring (LTR) transfer line to be transported to the electron

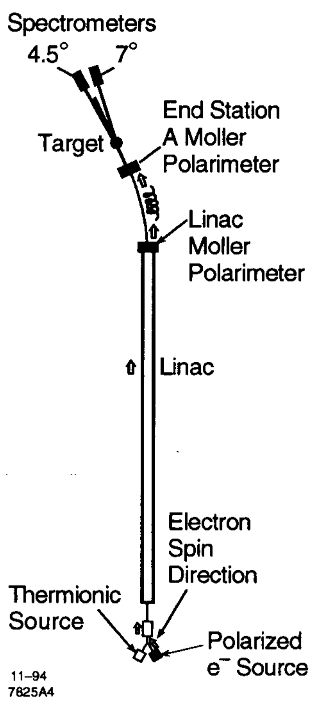

Figure 4. Polarized ESA operation.

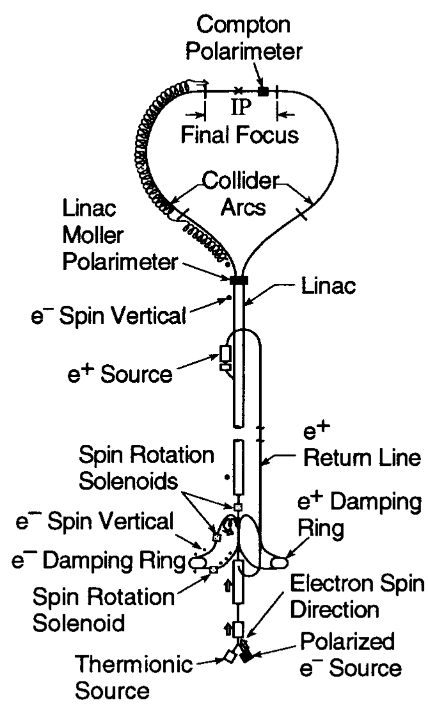

Figure 5. Polarized SLC operation.

damping ring (DR). The DR stores the beam for 8 ms to reduce the beam emittance. The ring-to-linac (RTL) transfer line transports the two bunches from the DR and a pulsed magnet kicks them back into the linac. These two bunches are preceded down the linac by a positron bunch which has been extracted from the positron DR. Three bunches are then accelerated down the linac. The trailing electron bunch is accelerated only to 30 GeV, and is then sent to the positron production target. Positrons in the energy range 2–20 MeV are collected, accelerated to 200 MeV, and transported to near the start of the linac for transport to the positron DR, where they are damped for 16 ms. At the end of the linac, the electron and positron energies are each 46.6 GeV. A magnet deflects the electron (positron) bunch into the north (south) collider arc for transport to the interaction point (IP). In the arcs, the beams lose about 1 GeV in energy from synchrotron radiation so that the resulting center-of-mass collision energy is 91.2 GeV, which is chosen to match the Z^0 mass. The beam energies are measured with energy spectrometers[23] to a precision of 20 MeV.

The electron spin orientation is longitudinal at the source and remains longitudinal until the LTR transfer line to the electron DR. In the LTR, the electron spin precesses by 450° to become transverse at the entrance to the LTR spin rotator solenoid. This solenoid rotates the electron spin to be vertical in the DR to preserve the polarization. The spin orientation is vertical upon extraction from the DR; it remains vertical during injection into the linac and during acceleration to 46.6 GeV down the linac. The spin transmission of this system is 0.99, with the small loss resulting from the beam energy in the DR being 1.19 GeV, slightly lower than the design energy of 1.21 GeV; this causes the spin precession in the LTR to be 442° rather than 450°, and the spin transmission is the sine of this angle.

The SLC arc transports the electron beam from the linac to the IP and is comprised of 23 achromats, each of which consists of 20 combined function magnets. At 46.6 GeV, the spin precession in each achromat is 1085°, while the betatron phase advance is 1080°. The SLC arc is therefore operating near a spin tune resonance. A result of this is that vertical betatron oscillations in the arc's achromats (combined function magnets that bend the beam in the horizontal plane), can cause the beam polarization to rotate away from vertical; this rotation is a cumulative effect in successive achromats. (The rotation of the vertical spin component in a given achromat is simply due to the fact that rotations in x and y do not commute, while the cumulative effect is due to the spin resonance.) The resulting spin component in the plane of the arc then precesses significantly.

The arc's spin tune resonance, together with misalignments and complicated rolls in the arc,[24] result in an inability to predict the spin orientation at the IP for a given spin orientation at the end of the linac. However, we have two good experimental techniques for orienting the spin longitudinally at the IP. First, using the RTL and linac spin rotator solenoids, one can orient the electron spin to be along the x, y, or z axis at the end of the linac. The z-component of the arc's spin transport matrix can then be measured with the Compton polarimeter, which measures the longitudinal electron polarization as described below. The Compton measures

$$P_z^C = R_{zx} \cdot P_x^L + R_{zy} \cdot P_y^L + R_{zz} \cdot P_z^L \tag{1}$$

The experimental procedure is referred to as a three-state measurement, and is accomplished by measuring P_z^C for each of x, y, or z spin orientations at the end of the linac. Using equation (1), the arc spin rotation matrix elements R_{zx}, R_{zy}, R_{zz} are then determined. This is sufficient to determine the full rotation matrix, which is described by three Euler angles. The matrix R can then be inverted to determine the required spin orientation at the end of the linac for the desired longitudinal orientation at the IP. This linac spin orientation is achieved with appropriate settings of the RTL and linac spin rotators.

Table II: Beam Parameters for SLC Operation

Parameter	1993	1994 (expected)
N^+	$3.0 \cdot 10^{10}$	$3.5 \cdot 10^{10}$
N^-	$3.0 \cdot 10^{10}$	$3.5 \cdot 10^{10}$
f_{rep}	120 Hz	120 Hz
σ_x	0.8 μm	0.5 μm
σ_y	2.6 μm	2.4 μm
Luminosity	$5 \cdot 10^{29}$ cm^{-2}s^{-1}	$1 \cdot 10^{30}$ cm^{-2}s^{-1}
Z/hr (peak)	50	100
Collision energy	91.26 GeV	91.26 GeV
Polarization	63%	80%
Up time	70%	70%
Run time	6 months	7 months
Integrated Zs	50 K	100 K

A second method to orient the spin longitudinally at the Compton takes advantage of the arc's spin tune resonance. A pair of vertical betatron oscillations (spin bumps), each spanning seven achromats in the last third of the arc, are introduced to rotate the spin.[25] The amplitudes of these spin bumps are empirically adjusted to achieve longitudinal polarization at the IP. Experiments have verified that the two spin orientation techniques provide consistent results to a precision of about 1% in the longitudinal IP polarization. Thus, the two spin bumps can effectively replace the two spin rotators. This turns out to be very important for SLC operation, where high luminosity has been achieved by producing and colliding flat beams (see Table II). Flat beams are naturally produced in the damping rings if the x and y betatron tunes are different. Preserving the flat beams during acceleration and transport to the IP requires minimizing any x-y coupling in the accelerator. The coupling introduced by the RTL and linac spin rotator solenoids proves to be unacceptable. So the *problem* of the arc spin tune resonance for modeling the arc spin transport has become a *feature* that allows both spin orientation control and flat-beam running for high luminosity.

3. Polarimetry

Three different polarimeter techniques are used at SLAC; these techniques are based on Mott scattering, Moller scattering, and Compton scattering. The ESA experiments rely on Moller polarimeters, while the SLD experiment relies on a Compton polarimeter. Mott polarimeters are used in test labs for polarized gun development work and for photocathode R&D. A considerable amount of work has been done and is continuing to be done at SLAC to compare results from the different polarimeters, and this will be discussed below. Comparing the results requires a degree of caution, since the polarization of a cathode has been observed to have significant dependencies on the cathode QE and the thickness of the strained layer. Also, different cathodes with similar properties may exhibit different polarization characteristics, especially if they are from different wafers. Both the E143 and the SLD experiments have utilized the strained lattice cathodes. Because E143 does not require much peak current, it can run with much lower cathode QE than the SLD experiment. This provides as much as 5 to 10% higher relative polarization for E143. For E143 and for the 1994 run of the SLD experiment, strained-lattice cathodes of thickness 0.1 μm are used. The 1993 SLD run, however, used an 0.3 μm-thick strained lattice cathode. The strain in the thicker cathode partially relaxes, and results in a polarization of about 65% compared to about 80% for the thinner cathode (as determined by the Compton polarimeter during SLD running). With these considerations in mind, let us consider the different SLAC polarimeters.

<u>Mott Polarimeters.</u> Mott polarimeters utilize the spin-dependent cross-section asymmetry in the elastic scattering of polarized electrons from an unpolarized high Z nucleus.[26] SLAC has three Mott polarimeters; all are in test labs. The first one is PEGGY, which is being used for R&D on high-polarization cathodes. PEGGY was used in the parity violation experiments at SLAC in the late 1970s, and was calibrated against a Moller polarimeter at that time. A newer polarimeter is SLAC's cathode test system (CTS) Mott,[27] which was built and calibrated at UC Irvine.[28] Following the 1993 SLD run, the cathode for that run was measured by the CTS polarimeter to give $P_e = (64 \pm 2)\%$. This would give $P_e \sim 62\%$ at the SLD IP, given spin transport losses in the DR and the arc. A third Mott polarimeter is now installed in SLAC's polarized gun test system (GTS), which is a mockup of the polarized source. This Mott is currently being commisioned. The PEGGY Mott and the GTS Mott use an energy filter to select elastically scattered electrons, while the CTS is a more precise retarding-field Mott. SLAC's polarized source group (in collaboration with other labs at Rice University, UC Irvine, University of Nebraska and Nagoya University) is currently undertaking a program to cross-calibrate these Mott polarimeters using a standard cathode. This standard cathode is chosen to be an 0.1 μm thick active layer of unstrained GaAs. Using the standard cathode, the calibration of SLAC's CTS Mott has been re-checked against the UC Irvine Mott and found to be consistent within the quoted 2% uncertainty.

<u>Moller Polarimeters.</u> SLAC's Moller polarimeters[29] measure the elastic scattering cross-section asymmetry in the collision of polarized beam electrons with polarized electrons in a magnetized permendur foil (49% iron, 49% cobalt, 2% vanadium). The linac Moller polarimeter is a single-arm device, detecting only the scattered beam electrons. This polarimeter is used as a diagnostic for both SLC and ESA operation. A schematic of it is shown in Figure 6. The ESA Moller polarimeter consists of both a single-arm Moller, and a double-arm Moller, which detects both the scattered beam electrons and the scattered target electrons. Unlike the Compton polarimeter described below, Moller polarimeter operation is not compatible with normal data taking, and special runs are needed. For the ESA experiments, polarimeter runs typically take 30 to 60 minutes to achieve 1% statistical

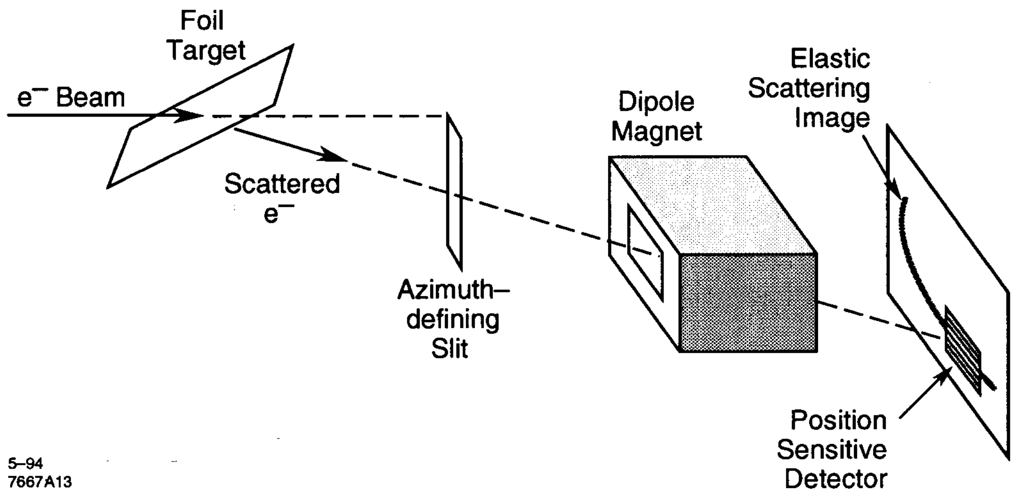

Figure 6. Moller Polarimeter.

precision, and are scheduled once per day.

The Moller polarimeters measure the cross-section asymmetry for beam and target spins aligned versus anti-aligned, and the asymmetry is proportional to the product of the beam and target polarizations. The target polarizations are typically about 8% (iron has two electrons out of 26 polarized) resulting in a small measured asymmetry. The uncertainty in the target polarization (about 3% relative) represents the largest systematic error in the measurement.

A large discrepancy between the beam polarization in the linac measured by the linac Moller and that inferred from the SLD Compton after small corrections for spin diffusion in the arc was discovered during the 1993 SLD run. The Compton measurements implied that $P^{linac} = (65.7 \pm 0.9)\%$, while the initial Moller results gave $P^{linac} \sim 80\%$. This discrepancy actually delayed the announcement of SLD's precise A_{LR} measurement by about 6 months until the discrepancy could be resolved.

Resolution of this discrepancy came from a correction to the Moller polarization analysis. This correction required proper accounting for the effect of atomic momenta of the electrons in the Moller target (the Levchuk Effect).[30] The atomic momentum of the inner K-shell electrons in an iron nucleus is about 100 keV/c. This is small compared to the 46.6 GeV beam energy, but not so small compared to the electron mass. Proper treatment of the relativistic scattering kinematics for the linac Moller geometry revealed that this small atomic momentum significantly broadened the elastic Moller peak in the high resolution silicon strip detector.

The polarized electrons in the target are outer-shell electrons, which have a small binding energy and hence do not cause a significant broadening of the Moller peak. The unpolarized inner-shell electrons, however, do cause a significant broadening. Thus the observed Moller line shape in the detector is broader than what would be observed if the target electrons were free, and the observed Moller asymmetry in the center of the Moller peak is greater. A proper analysis of the linac Moller data then gave $P^L = (69 \pm 3)\%$, which is consistent with the Compton result,[31] and the χ^2 of the line shape agreement between the montecarlo and data improved by about a factor of 10.

The large 15% (relative) correction in the linac Moller analysis due to the Levchuk effect does *not* imply a large universal correction for all Moller polarimeters. The correction depends on geometrical details of the polarimeter and also on electron beam characteristics. The correction is particularly large for the linac Moller due to its fine resolution and also the low emittance of the SLC beam. Double arm polarimeters, for example, tend to have large acceptance and poor resolution and this effect can be negligible. Such is the case for the ESA double arm Moller polarimeter. For E143, it measured an average beam polarization of $(84 \pm 3)\%$. This result is consistent with the preliminary SLD Compton result of about 80%, and is somewhat higher due to the lower cathode QE that E143 can accommodate.

Compton Polarimeters. The longitudinal electron beam polarization ($\mathcal{P}_e$) at the SLC IP is measured by the Compton polarimeter[32] shown in Figure 7. This polarimeter detects Compton-scattered electrons from the collision of the longitudinally polarized electron beam with a circularly polarized photon beam. The photon beam is produced from a pulsed Nd:YAG laser operating at 532 nm. After the Compton Interaction Point (CIP), the electrons pass through a dipole spectrometer; a nine-channel Cherenkov detector then measures electrons in the range 17 to 30 GeV.

The counting rates in each Cherenkov channel are measured for parallel and anti-parallel combinations of the photon and electron beam helicities. The asymmetry formed from these rates is given by

$$A(E) = \frac{R(\rightarrow\rightarrow) - R(\rightarrow\leftarrow)}{R(\rightarrow\rightarrow) + R(\rightarrow\leftarrow)} = \mathcal{P}_e \mathcal{P}_\gamma A_C(E)$$

where $\mathcal{P}_\gamma$ is the circular polarization of the laser beam at the CIP, and $A_C(E)$ is the Compton asymmetry function. The laser is polarized with a linear polarizer and a Pockels Cell, similarly to the way it is done for the polarized electron source. Measurements of $\mathcal{P}_\gamma$ are made before and after the CIP. By monitoring and correcting for small phase shifts in the laser transport line, we are able to achieve $\mathcal{P}_\gamma = (99 \pm 1)\%$. The unpolarized Compton cross-section and $A_C(E)$ are shown in Figure 8. The Compton spectrum is characterized by a kinematic edge at 17.4 GeV (180° backscatter in the center-of-mass frame), and the zero-asymmetry point at 25.2 GeV (90° backscatter in the center-of-mass frame). The Compton asymmetry function is modified from the theoretical asymmetry function[33] by detector resolution effects. This effect is about 1% for the Cherenkov channel at the Compton edge. Detector position scans are used to precisely locate the Compton edge. The position of the zero-asymmetry point is then used to fit for the spectrometer dipole bend strength. Once

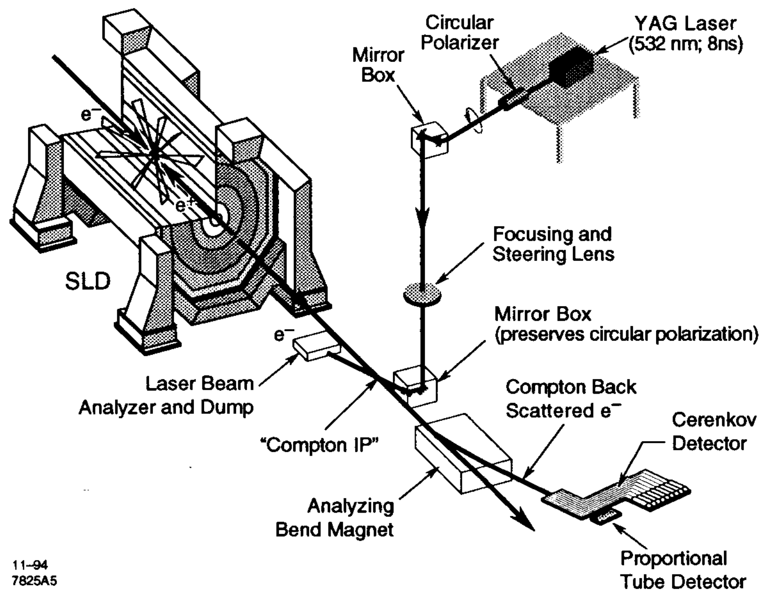

Figure 7. SLD Compton polarimeter.

the detector energy scale is calibrated, each Cherenkov channel provides an independent measurement of $\mathcal{P}_e$. The Compton edge is in channel 7, and we use this channel to precisely determine $\mathcal{P}_e$. The asymmetry spectrum observed in channels 1 to 6 is used as a cross check; deviations of the measured asymmetry spectrum from the modeled one are reflected in the inter-channel consistency systematic error (see Table III). Figure 9 shows the good agreement achieved between the measured and simulated Compton asymmetry spectrum for the 1993 SLD run. As an example of raw online data from the polarimeter, Figure 10 shows the signal height in ADC counts from channel 7 for 100 consecutive triggers. This data was taken during commissioning for the 1994 run. The polarimeter data acquisition was running at 30 Hz, the electron beam was present at 10 Hz, and compton collisions occurred at 5 Hz. Clearly evident are the pedestal (no electrons), the background (electrons, but no laser), and the $J = 1/2$ and $J = 3/2$ compton signals. This data corresponds to $P_e \sim 80\%$.

Polarimeter data are acquired continually during the operation of the SLC. The absolute statistical precision attained in a three-minute interval is typically $\delta\mathcal{P}_e < 1.0\%$. The systematic uncertainties that affect the polarization measurement are summarized in Table III for the 1993 run, where the IP beam polarization averaged over the run was found to be $< P_z^{IP} >= (61.9 \pm 0.8)\%$. For the 1994 run, we expect the polarization to be close to 80%, and with a somewhat smaller uncertainty than in 1993.

A second Compton polarimeter at SLAC is being commissioned in the Final Focus Test Beam (FFTB) at the end of the linac. This polarimeter utilizes the laser and detector systems for experiment E144,[34] and analyzes both the Compton-scattered gammas and

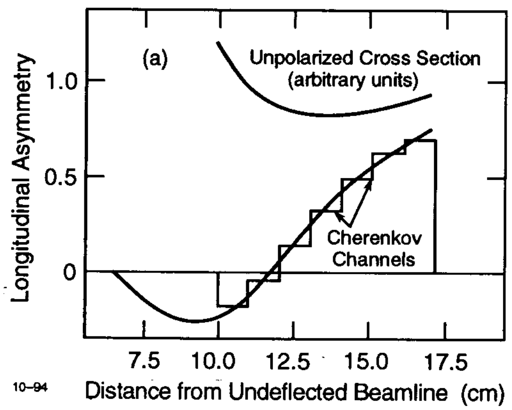

Figure 8: Compton cross section and asymmetry.

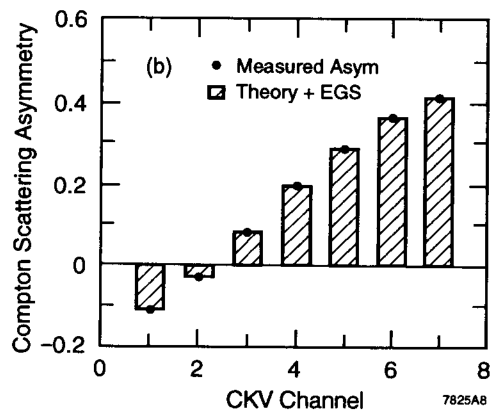

Figure 9: Measured and simulated Compton asymmetry.

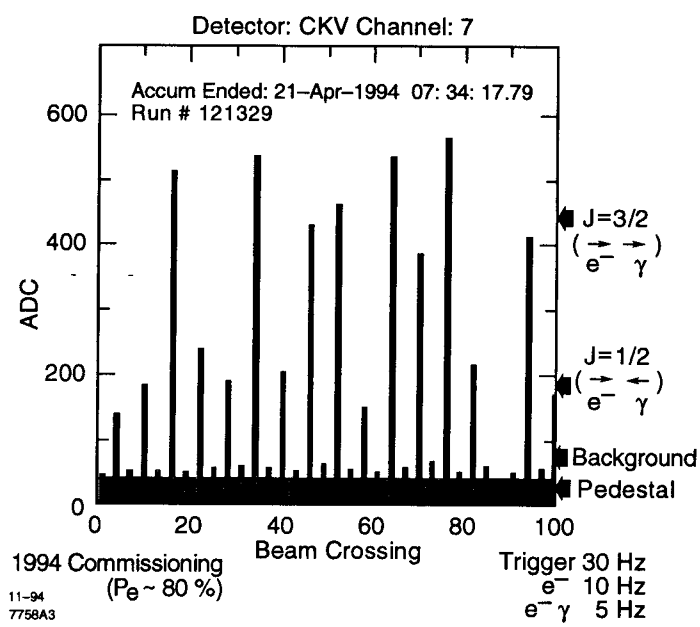

Figure 10: Online data from SLD Compton Cherenkov detector.

electrons using silicon-tungsten calorimeters. A first test run was completed in May 1994 and a second run should occur before spring 1995.

Table III: Systematic Uncertainties for the SLD Compton Polarimeter

Systematic Uncertainty	$\delta\mathcal{P}_e/\mathcal{P}_e$ (%)
Laser Polarization	1.0
Detector Calibration	0.4
Detector Linearity	0.6
Interchannel Consistency	0.5
Electronic Noise	0.2
Total Polarimeter Uncertainty	1.3

SUMMARY

Two years ago at the SPIN92 conference in Nagoya, Japan, SLD had just completed a physics run with $P_e = 22\%$, and E142 was about to start its physics run with $P_e = 40\%$. As of SPIN94 in Bloomington, IL, SLD is in the midst of a physics run with $P_e = 80\%$, and E143 has completed its physics run with $P_e = 84\%$. This high polarization is a tremendous accomplishment and has greatly enhanced SLAC's physics program. SLAC is now able to deliver a wide range of beam parameters with $P_e = 80\%$, including up to 6 amps of peak current.

Polarized source operation at SLAC has become routine, achieving up times of > 95% for roughly 5000 operating hours per year. This is encouraging the design of a polarized source for the next generation of linear colliders.[35] But the work for our polarized source colleagues is not yet finished. The beam polarization is still only 80-85%; they should now strive for 95-100%!

In End Station A, E154 and E155 are scheduled to run in 1995 and 1996 respectively. These experiments will further elucidate the spin structure of the nucleon. With the SLAC linear collider, the SLD experiment is scheduled to run through 1998, producing more precise measurements of parity violation in the Z-fermion couplings. SLD will continue to provide (and improve on) the world's best measurement of the weak mixing angle; and together with other precision electroweak experiments, will continue the experimental assault on the MSM.

REFERENCES

1. See, for example, F. E. Close, in *An Introduction to Quarks and Partons* (Academic Press Inc., 1979), p. 233.
2. M. J. Alguard et al., *Phys. Rev. Lett.* **37**, 1261 (1976).
3. G. Baum et al., *Phys. Rev. Lett.* **51**, 1135 (1983).
4. J. Ashman et al., *Nucl. Phys.* **B328**, 1 (1989).
5. J. Ellis and R. L. Jaffe, *Phys. Rev.* **D9**, 1444 (1974).
6. See, for example, R. L. Jaffe and A. Manohar, *Nucl. Phys.* **B337**, 509 (1990).
7. J. D. Bjorken, *Phys. Rev.* **148**, 1467 (1966); *Phys. Rev.* **D1**, 1376 (1970).
8. P. L. Anthony et al., *Phys. Rev. Lett.* **71**, 959 (1993).
9. The E143 proton results can be found in K. Abe et al., SLAC-PUB-6508, August 1994; submitted to *Phys. Rev. Lett.*. See also presentations to this conference by D. Day, A. Feltham, and H. Borel.
10. B. Adeva et al., *Phys. Lett.* **B302**, 533 (1993).
11. D. Adams et al., *Phys. Lett.* **B329**, 399 (1994).
12. For a recent review of the experimental data, see J. Ellis and M. Karliner, CERN-TH-7324, July 1994.
13. Presentations to this conference were given by M. Woods and K. Pitts. See also K. Abe et al., SLAC-PUB-6607, submitted to *Phys. Rev. Lett.*; K. Abe et al., SLAC-PUB-6644, submitted to *Phys. Rev. Lett.*; K. Abe et al., SLAC-PUB-6605, submitted to *Phys. Rev. Lett.*
14. K. Abe et al., *Phys. Rev. Lett.* **73**, 25 (1994).
15. The weak mixing angle describes the mixing of the neutral $SU(2)_L$ and U(1) gauge bosons to form the physical γ and Z^0. Due to radiative corrections, there are different conventions for defining this angle. We follow the convention for $\sin^2\theta_W^{\rm eff}$ as used by the LEP collaborations, which is given in *Phys. Lett.* **B276**, 247 (1992).
16. For recent reviews of tests of the MSM, see M. Swartz, SLAC-PUB-6384, November 1993; and A. Blondel, CERN-PPE/94-133, August 1994.
17. A detailed description of SLAC's polarized electron source can be found in R. Alley et al., SLAC–PUB–6489, January 1995; to be submitted to Nucl. Inst. Meth.
18. K. Witte, SLAC-PUB-6443, March 1994.
19. J. Frisch, R. Alley, M. Browne, M. Woods, SLAC-PUB-6165, April 1993.